Science and Technology for Energy Transition **79**, 49 (2024)

https://doi.org/10.2516/stet/2024044

Available online at:
stet-review.org

Decarbonizing Energy Systems: Smart Grid and Renewable Technologies
Fang Rui-ming and Qiangqiang Liao (Guest Editors)

REGULAR ARTICLE OPEN ACCESS

Energy management strategy of microgrid based on photovoltaic and energy storage system in construction area of Sichuan-Tibet Railway

Na Shu[1], Shan Jiang[1], Zhongze Fan[1], Xiaoman Cao[1], and Zeling Zhang[2,*]

[1] Shandong Electric Power Engineering Consulting Institute Corp., LTD, Shandong 250100, China
[2] Anhui Nenghui Rail Transit Technology Co., Ltd, Ma'anshan 243071, China

Received: 3 March 2024 / Accepted: 11 June 2024

Abstract. The construction area of the Sichuan-Tibet Railway is located at a high altitude with thin air conditions, but it benefits from excellent solar irradiance. To address issues such as insufficient power and low efficiency of traditional fuel-based equipment in such harsh environments, electric equipment is being employed as a replacement for conventional fuel-based equipment. In order to achieve sustainable development for the Sichuan-Tibet Railway, this article proposes that a microgrid can be conducted in the construction area of the Sichuan-Tibet Railway which will provide power to the electric equipment during the construction process and to electric locomotives upon completion. This article compares the characteristics of AC microgrids and DC microgrids, analyses and simulates the mathematical model of key converters, and introduces their control strategies. This article adopts a hybrid AC-DC microgrid for research purposes and proposes a time-period-controlled energy management strategy for the photovoltaic-storage hybrid AC-DC microgrid in the construction area of the Sichuan-Tibet Railway. The simulation results demonstrate that the AC-DC microgrid in the construction area based on the proposed time-period-controlled energy management strategy could effectively meet the load demands of different time periods and provide power to the electric equipment used in the construction area of the Sichuan-Tibet Railway.

Keywords: Microgrid, Photovoltaic, Energy storage, Electric equipment.

1 Introduction

The goals set by the United Nations and the Paris Agreement limit the global temperature rise to under 1.5 °C from the preindustrial levels by the end of this century. To achieve this goal, a reduction of CO_2 emissions to zero is necessary, either by completely eliminating the carbon emissions from the energy industries and processes or by offsetting the remaining emissions using carbon dioxide removal technologies [1]. China has actively responded to this by embracing the goal of "carbon peak and carbon neutrality" and implementing the new development philosophy to establish a new development paradigm. Under the vision of achieving the dual goals of "carbon peak and carbon neutrality," the demand for decarbonization and carbon reduction in the transportation sector is growing. The electrification of the construction area in Section 10 of the Sichuan-Tibet Railway, upon which this article is based, is one significant measure in this regard.

High-speed trains are a type of equipment utilizing advanced technology and complex structures [2]. Today, most European countries, Russia, Japan, and China have constructed their complex high-speed railway networks [3]. But only a few countries have built high-speed railways in the highlands. The construction of the Sichuan-Tibet Railway is currently underway, and auxiliary tunnels such as inclined shafts and adits are being built in much greater length than the main line. A large quantity of tunnel construction equipment, including rock drilling rigs and excavators, needs to be deployed. The construction area of the Sichuan-Tibet Railway experiences thin air due to the high altitude and plateau environment. Traditional fuel-powered construction equipment commonly faces issues such as reduced power output, increased energy consumption, and intensified emission pollution. These issues are particularly prominent during long-distance tunnel construction. Furthermore, safety hazards such as competition for oxygen among workers and the accumulation of harmful gases exist. However, the construction area is abundant in renewable energy sources such as water, solar power, and

* Corresponding author: 2180797984@qq.com

geothermal energy. Among these clean energy sources, solar is the main contributor to the increase in the share of renewable energy [4].

The new energy construction equipment industry, exemplified by electric excavators, is in its early developmental stage, with immature supporting technologies such as battery drive and limited product variety. Currently, a small number of electric equipment has been utilized in the construction of the Sichuan-Tibet Railway tunnel for trial purposes.

To facilitate the continuous promotion and widespread adoption of new energy-green construction equipment, power supply technology specific to the construction area of plateau railways must be developed. The microgrid (MG) is a promising technology to tackle the challenges arising from renewable energy integration and to improve energy efficiency in the power grids [5]. The development and expansion of microgrids can effectively facilitate the large-scale integration of distributed power and renewable energy, ensuring the reliable supply of various energy forms to loads. Therefore, the introduction of microgrids is essential in the process of construction of the Sichuan-Tibet Railway.

The Sichuan-Tibet Railway is a high-speed railway in China that connects Sichuan Province with the Tibet Autonomous Region. It runs from east to west, starting from Chengdu in Sichuan Province and ending in Lhasa, the capital city of Tibet Autonomous Region. It is the second railway line to reach Tibet and is also one of the main railway lines in southwest China. The research in this article is based on the CZXZZQ-10 section of the Sichuan-Tibet Railway, which refers to the Changdu to Bomê segment.

The CZXZZQ-10 section is located in the Karuo District of Changdu City and Basu County in the Tibet Autonomous Region. The total length of this section is 41.832 km, and the construction scope extends from the 2nd inclined shaft of the Bangda Tunnel to the 1st inclined shaft of the Gula Mountain Tunnel. The average elevation is about 4400 m, with the highest point at 4575 m (1st inclined shaft of Gula Mountain). The on-site construction of the CZXZZQ-10 section of the Sichuan-Tibet Railway involves two major scenes: tunnels and bridges. Tunnels are the main focus, with a total tunnel length of 27.55 km (accounting for 65.9% of the section length), including a 17.25-kilometer-long Bangda Tunnel and a 10.29-kilometer-long Gula Mountain Tunnel. The bridges have a total length of 7576.5 m (4 bridges, accounting for 18.1% of the section length), with 11 culverts. The section also includes 77.8 km of track, 250 prefabricated box girders (Bangda Bridge), and one station (Bangda Station).

This article describes the solar irradiance and the application of electrification equipment in the construction area of the Sichuan-Tibet Railway. This article summarizes and compares the characteristics of different forms of microgrids, analyzes the mathematical model of key converters and control strategies in microgrids, and based on the analysis, establishes a simulation of an AC/DC microgrid. The highlights of this article are twofold. Firstly, the use of microgrids in the construction area of the Sichuan-Tibet Railway located on the plateau to provide power for electrification equipment, aiming to achieve sustainable construction practices. Secondly, the proposal of a time-based control energy management strategy for the photovoltaic energy storage AC/DC microgrid in the construction area of the Sichuan-Tibet Railway.

2 Construction scenario

2.1 Solar resource

CZXZZQ-10 section of the Sichuan-Tibet Railway is located within the territory of Tibet. Tibet is one of the regions in China with abundant solar irradiance resources. According to [4], over the past 30 years (1991–2020), Tibet has had an average global horizontal irradiance of 1816 kWh/m^2, with the highest annual level reaching 2189 kWh/m^2. The total irradiance is highest in May and lowest in December. To calculate the theoretical energy based on solar radiation reaching the Earth's surface, equations (1) and (2) can be used. The annual irradiation amount of all grid points in the evaluation area is added. Multiply the result to the grid point area. The annual theoretical total amount of solar energy resources S_E in the evaluation area (kWh, MJ, standard coal) can be obtained. Then S_E is divided by the year-round time to obtain the annual average theoretical total amount of solar energy resources S_P in the evaluation area in the unit of power (kW) [4]. The equation is as follows:

$$S_E = \sum\nolimits_{i=1}^{n} S_i \cdot A_i \tag{1}$$

$$S_P = \frac{S_E}{T} \tag{2}$$

In equation (1), S_i is the annual radiation dose per grid point in kWh/m^2, A_i is the area of each grid. The data used in this study are equal grid spacing of 1 km resolution, and the area of all grid points is 1 km^2. n is the number of grid points in the evaluation area, T is the annual hours, namely 8760 h.

In terms of the theoretical total amount within the regional area, the annual global horizontal radiation of the whole region is 240.07 billion tons of standard coal or 222.91 billion kW on average.

Given the abundant solar irradiance resources in the Tibet region, a corresponding photovoltaic (PV) power system has been constructed in the construction area of the CZXZZQ-10 section of the Sichuan-Tibet Railway. It is possible to estimate the theoretical annual electricity generation for the CZXZZQ-10 section based on the peak sun hours and installed capacity.

$$E_P = H \cdot P \cdot K \tag{3}$$

In equation (3), P represents the installed capacity of the system (kWp), and H represents the local peak sun hours (h). For Changdu, H is 4.91 h, and for Bomê, it is 4.81 h. In equation (3), taking the average value of 4.86 h. K represents the system's overall efficiency (typically ranging from 75% to 85%, here we assume 80%). According to equation (3), the theoretical annual photovoltaic electricity generation for the CZXZZQ-10 section of the Sichuan-Tibet Railway can reach $992.8*10^3$ kWh. [6] introduces a study on using machine learning to predict solar power generation, where random Forest Regression Regression (RFR) and Long Short-Term Memory (LSTM) models outperformed the other models. This research contributes to the accurate prediction of photovoltaic generation within the construction area. Equation (3) mentioned above represents the average model for photovoltaic generation prediction, which can only provide an approximate estimation of the annual total power generation and may lack precision. However, by incorporating environmental factors, as shown in equation (4), reference can be made to the methods outlined in [6] for predicting photovoltaic generation.

$$E_P = H \cdot P \cdot K \cdot T_c \cdot S_c \cdot L_c \tag{4}$$

where T_c the temperature correction factor, S_c is the Shading Correction Factor, L_c is the System Loss Correction Factor, and H, P, and K parameters are equal to equation (3).

2.2 Electric equipment

In the construction area of the CZXZZQ-10 section, a portion of electric equipment has been implemented. In terms of loaders, there are representatives such as XC968-EV and XC975-EV, which are the epitome of Xuzhou Construction Machinery Group (XCMG) ‘s third-generation pure electric loaders. They adopt the industry’s pioneering “three-motor” technology, eliminating the need for a gearbox in the entire machine. By utilizing XCMG’s core proprietary power intelligent matching and optimization technology, the integrated intelligent control of motor power, speed, and torque is achieved. This, combined with functions such as an intelligent thermal management system, energy recovery, and three-level fault safety protection, enables intelligent, efficient, and safe operation of the whole machine. These loaders can be widely used in various working conditions such as steel plants, power plants, coking plants, the coal chemical industry, coal yards, sand and gravel materials, and tunnels, meeting the environmental usage requirements from −40 °C to 50 °C. They support DC fast charging and can also be charged with a single gun. The charging power ranges from 240 kW to 360 kW, providing a general endurance of 6–8 h. The average energy consumption cost is only one-third of that of a diesel engine, significantly reducing energy usage costs. The specific parameters of the XC series electric equipment are shown in Table 1.

In the CZXZZQ-10 section, the drilling and blasting method will be predominantly used, with blasting and excavation as the primary methods. Loaders (XC series) and excavators will be used to transport rocks and debris inside the tunnel. Self-dumping trucks will be used for transportation, and concrete mixing trucks will transport concrete for spraying and reinforcement of the tunnel walls. One cycle takes approximately 16 h. With the exception of special circumstances such as power grid maintenance or extreme weather conditions, the tunnel construction will be carried out continuously throughout the year, with 24-h uninterrupted operations. The transportation distance for construction vehicles on each working face is relatively short, with a one-way distance not exceeding 10 km. The main construction process of the tunnel is shown in Table 2.

Table 1. XC968/975-EV parameters.

Projects	XC968-EV	XC975-EV
Rated bucket capacity (m^3)	2.5–5.5	3.5–5.0
Rated load (kg)	6000	7000
Rated power (kW)	270	270
Maximum digging force (kN)	≥180	195

Table 2. Construction process.

Number	Process	Time-consuming(h)
1	Drilling and blasting	4
2	Transportation of waste	4
3	Erecting scaffolding	4
4	Sprayed concrete	4
5	Sum	16

Based on on-site testing of electric vehicles, the energy consumption for electric dump trucks in the construction area is estimated to be around 4.2 kWh/km, while the energy consumption for electric concrete mixers is estimated to be around 3 kWh/km. Based on this information, a certain sub-tunnel is equipped with 5 electric dump trucks and 5 electric concrete mixers. Under the mentioned operating conditions, the annual energy consumption for the dump trucks in this sub-tunnel is approximately 400,100 kWh, and for the concrete mixers is approximately 93,100 kWh.

3 Structure of typical microgrid

The term ‘microgrid’ refers to the concept of a small number of new distributed energy resources (DER) connected to a single power subsystem. DER includes both renewable and/or conventional resources [7].

A microgrid can be architected to function either in grid-connected or standalone mode, depending upon the generation, integration potential to the main grid, and consumers’ requirements [8].

Considering the geography of high-altitude and cold regions, as well as the economic development status, the development and utilization of renewable energy based on local conditions is an inevitable trend for sustainable development. At present, various complementary renewable energy sources, distributed generation and grid control, microgrids, and other technologies have become relatively mature, providing a solution for the power supply issues in areas of high-altitude and cold regions, such as the construction area of the Sichuan-Tibet Railway. [9] Introduces

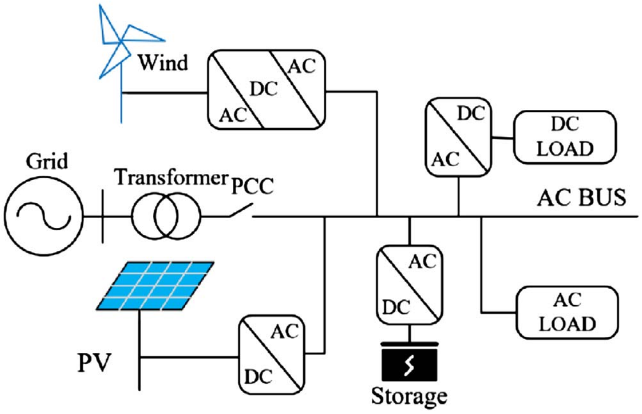

Figure 1. AC Microgrid structure.

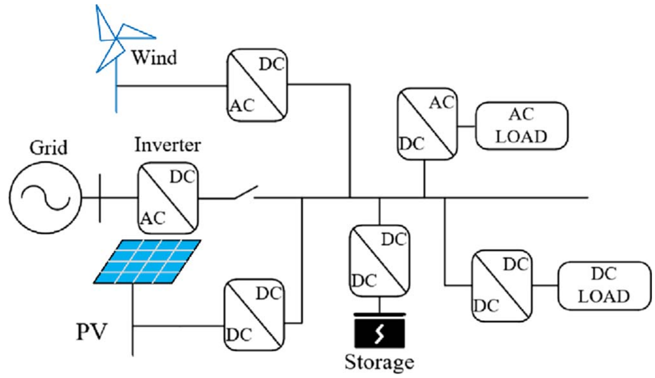

Figure 2. DC Microgrid structure.

the research status and development trends of intelligent distributed microgrid systems and analyzes the factors affecting the power generation efficiency of a 45.9 kW intelligent distributed photovoltaic microgrid system in the Energy Research and Demonstration Center of Tibet Autonomous Region. [10] provides an overview of the concept and characteristics of intelligent distributed microgrids, presents the current structure of their application in various countries, and analyzes the three key components of intelligent distributed photovoltaic microgrid systems (energy management, system control, and system protection). Both articles are based on the concept of intelligent distributed microgrids but focus on different aspects. [9] emphasizes the factors influencing power generation and conducts research on power generation, while [10] focuses on the system concept and introduces each component. Additionally, [11] analyzes the types of micro sources included in stand-alone photovoltaic microgrids in high-altitude mountainous regions, synthesizes the operation principles of microgrids, and provides corresponding models and control strategies.

According to the bus configuration, microgrids can be divided into AC microgrids, DC microgrids, and AC-DC microgrids. For example, in an AC microgrid, the bus operates on AC power. Within the AC microgrid, distributed power sources and energy storage devices are connected to the AC bus through power electronic devices. Distributed power sources are typically connected to the AC bus in the form of photovoltaic inverters and wind power AC/DC/AC converters, while energy storage devices are connected to the AC bus through bidirectional power converters to enable bidirectional energy flow. There is a Point of Common Coupling (PCC) between the AC bus and the main power grid, which allows for switching between off-grid and grid-connected modes. The typical structure of an AC power grid is shown in Figure 1. [12] proposes a constant power optical storage AC microgrid and studies the power and energy storage capacity of the system, with a focus on ensuring fixed generation within a specific time period under limited charging conditions.

AC microgrids do not require expensive converter stations as distributed power sources can be connected to the AC bus through power electronic devices. Additionally, AC microgrids have been developed earlier and the technology is relatively mature. However, AC microgrids have limited overcurrent capability and are significantly affected by the stability when subjected to large and sudden loads. Moreover, with the integration of photovoltaics, energy storage, and a significant amount of DC load, AC grids face challenges in energy coordination control, reduced stability, and increased construction costs.

In DC microgrids, distributed energy sources and storage devices are connected to the DC bus through power electronic devices. Typically, photovoltaic, fuel cells, and supercapacitors are connected to the bus through DC/DC converters, while wind power and flywheel energy storage are connected through AC/DC converters. Considering different voltage levels of DC loads, DC loads are connected to the DC bus through DC/DC converters, while AC loads are powered through inverters. Similarly, there is an inverter between the DC bus and the main power grid, enabling switching between grid-connected and island modes. The structure of a DC microgrid is illustrated in Figure 2. [13] introduces a three-layer control structure for a DC microgrid and compares it with an AC microgrid, demonstrating the advantages of DC microgrids. [14] focuses on the design of DC/DC converters in DC microgrids to enhance system reliability. These two articles provide valuable insights into the control structure and converter design of microgrids, which will be reflected in subsequent discussions on control structures

DC microgrids that have low line losses as they have minimal inductive losses and skin effects. They consist only of DC bus, which makes their control relatively easier since maintaining stable bus voltage ensures internal power balance. Additionally, power electronic conversion in DC microgrids is comparatively straightforward, as distributed power sources can be connected to the bus through DC/DC or AC/DC converters, reducing the need for numerous rectification and inversion processes. However, considering the intermittent and time-varying nature of distributed power generations, DC microgrids require higher coordination and control capabilities.

AC microgrids are a traditional form of power supply, and although they have become mature, they still have drawbacks such as complex control and multiple conversion stages. In comparison to AC microgrids, DC microgrids

Table 3. Comparisons of AC and DC microgrids.

Number	AC microgrids	DC microgrids
Operating efficiency	Multiple conversion stages, low efficiency	Few conversion stages, high efficiency
Control performance	Complexity in control	Flexibility in control
Operating cost	Low	High, requiring expensive devices
Power quality issues	Harmonics, frequency disturbances	Voltage ripple
Technology maturity	Highly mature	Developmental stage

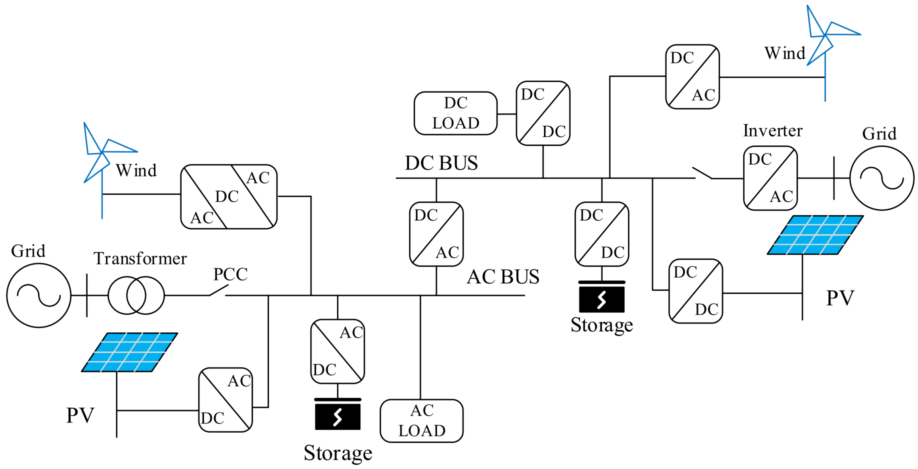

Figure 3. AC/DC Microgrid structure.

have gained increasing attention due to their simpler control, fewer energy conversion stages, and higher efficiency [15]. Detailed comparisons of AC and DC microgrids are shown in Table 3.

With the continuous development of microgrid technology, many scholars have proposed the integration of AC and DC microgrids, as shown in Figure 3, creating hybrid AC/DC microgrids [16, 17]. These microgrids combine the advantages of both AC and DC systems, reducing conversion stages, improving operational efficiency, and mitigating issues related to frequency and phase. They offer flexible control, high reliability for independent operation, and various benefits. [18] discusses the advantages and coordination control strategies of hybrid AC/DC microgrids, covering topics from distributed power sources to converter modeling and system coordination control. [19] introduces the topology of AC/DC microgrids and conducts reliability analysis. [20] primarily focuses on the control strategies for grid-connected and islanded modes in hybrid AC/DC microgrids, incorporating BP neural networks for power generation prediction. These three articles provide insights into hybrid AC/DC microgrids from different perspectives, with [18] emphasizing a macro-level overview, [19] focusing on topology and reliability analysis, and [13] highlighting the grid connection aspect.

The presence of AC bus and DC bus directly meets the requirements of AC or DC distributed generation units and mixed AC/DC loads, reducing unnecessary energy conversion stages to improve efficiency. The AC and DC buses can be independently controlled or coordinated, and the microgrid can also be connected to the distribution network, enabling grid-connected and islanded operation, greatly enhancing the reliability of the microgrid system. Hybrid AC/DC microgrid systems fully consider the characteristics of distributed generation units and the electrical demands and operational modes of loads, offering higher economic viability and reliability. As a result, they have found wide applications in engineering projects.

Considering the characteristics of the construction area of the Sichuan-Tibet Railway, which include thin air, weak environmental carrying capacity, abundant green power sources such as solar and hydroelectricity, as well as several challenges like limited electric equipment range, long charging times, high equipment costs, and difficulties in power supply assurance. From an energy perspective, photovoltaic generation produces DC electricity, which requires DC/DC conversion for efficient utilization, regardless of whether it goes through an inverter. The charging and discharging process of battery energy storage requires bidirectional DC/DC converters, allowing them to be connected to the DC bus simultaneously. In terms of loads, the DC bus in the hybrid AC/DC microgrid provides fast charging for electric equipment and supplies power to various DC loads. The AC bus provides power for traditional AC loads such as fans and air conditioners, while also supporting slow charging for electric equipment. In conclusion, adopting a hybrid AC/DC microgrid system is suitable for the construction area of the Sichuan-Tibet Railway.

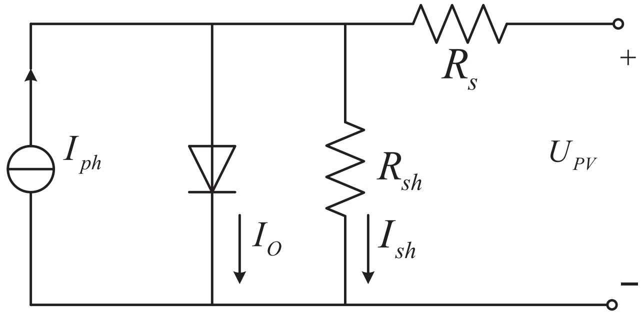

Figure 4. Equivalent circuit diagram of photovoltaic cell.

4 DERs and converters

4.1 Photovoltaic

The principle of photovoltaic power generation is to convert solar energy into electrical energy using the photovoltaic effect of semiconductor materials.

A typical photovoltaic power generation system consists of multiple photovoltaic cells, which are usually made of semiconductor materials such as silicon. When sunlight shines on the photovoltaic cell, the energy of photons (light quanta) is absorbed by the semiconductor material, causing electrons to be excited and generating electric current. This current can be collected and utilized through the circuit connected to the photovoltaic cell.

The photovoltaic cells convert energy by the "photo-generated voltage effect" which generates "photo-generated current" through an external circuit. The photovoltaic cell can be described by the equivalent circuit shown in Figure 4. To achieve higher voltage and power, photovoltaic cells are typically connected in series and parallel to form photovoltaic cell arrays or photovoltaic panels. Photovoltaic cell arrays can be combined into photovoltaic generation systems of different scales and power levels according to actual needs. These systems also include components such as controllers and inverters, which manage and convert the electrical energy generated by the photovoltaic cells for supply to the power grid or independent power supply.

In Figure 4, the relationship between output current I_{PV} and output voltage U_{PV} of photovoltaic cells is as follows:

$$I_{PV} = I_{ph} - I_o\{e^{\frac{q(U_{PV}+R_sI)}{T_{PV}AK}} - 1\} - \frac{U_{PV} + I_{PV}R_s}{R_{sh}} \tag{5}$$

In equation (4), I_{ph} is photo-generated current; I_o is diode reverse saturation current; q is the charge of the electron ($q = 1.6 \times 10^{-19}$ C); R_{sh} is equivalent resistance in parallel; R_s is the equivalent resistance in series; T_{PV} is the absolute temperature of the photovoltaic cell; A ($1 \leq A \leq 2$) is the ideal factor of diode; K is the Boltzmann constant ($K = 1.38 \times 10^{23}\ J/K$).

Environmental factors have a significant impact on the variable I_{ph} in equation (4), making it difficult to solve equation (4) with a simple mathematical model. Therefore, equation (4) lacks practicality. In engineering analysis, the output equation of a photovoltaic cell is typically calculated using parameters provided by the manufacturer, such as open-circuit voltage U_{oc}, short-circuit current I_{sc}, maximum power point voltage U_m, and current at the maximum power point I_m. The expression is as follows:

$$I_{PC} = I_{sc}\left[1 - C_1\left(e^{\frac{U_{PV}}{C_2U_{oc}}} - 1\right)\right] \tag{6}$$

$$C_1 = \left(1 - \frac{I_m}{I_{sc}}\right)e^{\frac{U_{PV}}{C_2U_{oc}}} \tag{7}$$

$$C_2 = \left(\frac{U_m}{U_{oc}} - 1\right)\Big/ ln\left(1 - \frac{I_m}{I_{sc}}\right) \tag{8}$$

where U_{oc} is open-circuit voltage, I_{sc} is short-circuit current, U_m is maximum power point voltage, and I_m is maximum power point. These parameters are standard condition parameters of the photovoltaic cell. C_1 and C_2 are correction parameters that account for environmental factors. When there are changes in solar irradiance and ambient temperature, it is common to make corrections using equations (8) and (9).

$$\Delta S_r = \frac{S_r}{S_{ref}} - 1 \tag{9}$$

$$\Delta T_r = T_r - T_{ref} \tag{10}$$

where S_r is the actual solar irradiance, T_r is the ambient temperature, S_{ref} is the reference solar irradiance and T_{ref} is the reference environmental temperature. Therefore, the expressions for U_{ocr}, I_{scr}, U_{mr}, and I_{mr} which are the actual values of U_{oc}, I_{sc}, U_m, and I_m are donated as:

$$\begin{cases} U_{ocr} = U_{oc}[(1 - \alpha\Delta T_r)ln(1 + \beta\Delta S_r)] \\ I_{scr} = I_{sc}(\Delta S_r + 1)(1 + \gamma\Delta T_r) \\ U_{mr} = U_m[1 - \alpha\Delta T_r]ln(1 + \beta\Delta S_r) \\ I_{mr} = I_m(\Delta S_r + 1)(1 + \gamma\Delta T_r) \end{cases} \tag{11}$$

where α, β, and γ are typically represented as $0.0025^\circ C$, 0.5, and $0.0028^\circ C$.

According to equation (10), photovoltaic power generation is influenced by both the inherent parameters of the photovoltaic cell itself and external environmental factors such as solar irradiance and temperature. When the environmental temperature is excessively high, the efficiency of photovoltaic cells decreases. [21] addressed this issue by optimizing the cooling system to enhance the efficiency of photovoltaic cells under high temperatures. This improvement is beneficial for future research aiming to enhance the efficiency of photovoltaics.

In the realm of microgrids, the prevalent approach for distributed photovoltaic power generation units is to employ maximum power tracking (MPPT) control. This method aims to optimize the utilization of distributed energy and prevent resource wastage. In the case of a photovoltaic power supply connected to the DC bus, the Boost circuit is utilized. Through MPPT control, the voltage is increased and connected to the DC bus. The control block diagram depicting the Perturbation and Observation method used in this article is illustrated in Figure 5.

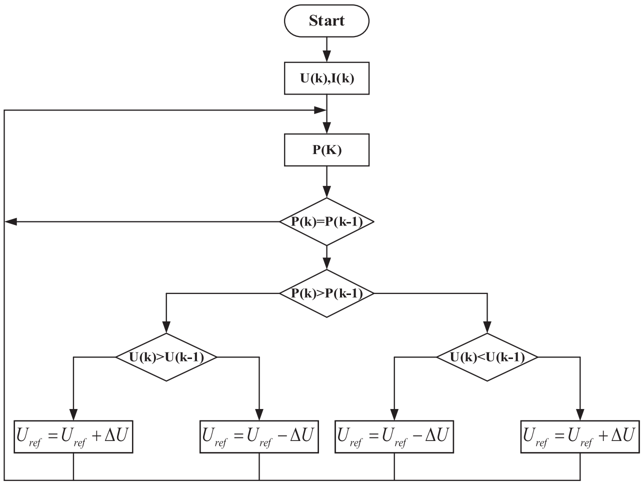

Figure 5. Perturbation and Observation Method.

4.2 Battery storage

Battery storage units facilitate energy exchange between batteries and microgrids through power electronic devices. These power electronic devices enable bidirectional energy flow, ensuring the dual operation of battery storage units. Additionally, in the event of a fault in the main power grid, battery storage units can serve as backup power sources for off-grid operation, supplying power to the loads in the system. In summary, battery storage units in photovoltaic battery storage microgrid systems serve several key functions. These include stabilizing the output of distributed photovoltaic sources, mitigating photovoltaic generation fluctuations, and smoothing the output curve. They also contribute to peak shaving and valley filling, considering the power consumption patterns of the main power grid, battery storage unit capacity, charging and discharging power, and daily load profiles. Furthermore, battery storage units can act as emergency backup power sources, ensuring the stable operation of the microgrid and continuous power supply to critical loads during the off-grid operation. They also enhance power quality by providing reactive power compensation to the main power grid, improving voltage stability, and reducing voltage fluctuations. Additionally, battery storage units can assist in load balancing and frequency regulation.

The mathematical model of a battery cell can be described using the equivalent circuit shown in Figure 6a. In the diagram, E represents the electromotive force of the power source, R_{bat} is the equivalent resistance that accounts for energy consumption during operation, C_b represents the equivalent capacitance between the positive and negative terminals, R_b is the contact resistance, and U_b is the output voltage of the battery. For the purpose of analysis, the battery model can be simplified by neglecting the capacitance, as shown in Figure 6b.

Battery storage units allow for a bidirectional flow of electrical energy, enabling both charging and discharging through control by power electronic devices. They can also serve as emergency backup power sources, supplying power to critical loads during off-grid operation of microgrid systems. When connected to the DC bus, battery storage units regulate power imbalances between the source and load, stabilizing the DC bus voltage. When connected to the AC bus, similar to photovoltaic sources, a two-stage control structure is employed. The front stage consists of a DC-DC control section that regulates the DC output, while the rear stage involves a DC-AC control section, which connects to the AC bus through LC filtering. In addition, battery state estimation is a crucial task in energy storage systems. [22] pointed out that conventional estimation methods based solely on battery terminal voltage have limitations. To address the limitations, a state estimation method utilizing neural networks is proposed, considering parameters such as battery terminal voltage, load current, battery temperature, and specific gravity of electrolyte. This method provides guidance for estimating the state of the battery in the system.

Whether connected to the AC bus or the DC bus, the DC/DC conversion section utilizes a bidirectional Buck/Boost converter. The basic operating principle of the bidirectional Buck/Boost converter is to achieve voltage conversion by selectively turning on and off two IGBTs while maintaining the polarity of the voltage at both ends of the converter, enabling bidirectional energy flow as required. Depending on the direction of energy flow, the Buck/Boost bidirectional converter can operate in either boost or buck mode to step up or step down the voltage [23].

The bidirectional Buck/Boost topology is shown in Figure 7. In Figure 7, V_1 and V_2 are respectively the input/output voltage, and the switching tubes S_1, S_2, D_1, and D_2 constitute a voltage rise and fall conversion circuit, which can meet the requirements of current flow in both forward and reverse directions. The low voltage V_1 of the DC power supply can be converted to the high voltage V_2 by controlling the switch tube periodically to turn on and off, and the load can be powered.

It is considered that the power imbalance between the source charges needs to be adjusted by the ability of energy storage or release, so as to control the DC bus voltage to reach a stable state. In the DC/DC conversion part of this article, the traditional voltage and current double close-loop control strategy is used to stabilize the bus voltage. Its control block diagram is shown in Figure 8. The control of the DC/AC part has been introduced in the inverter section above, and will not be repeated here. The output voltage of the bidirectional DC/DC converter is shown in Figure 9.

4.3 Inverter

The voltage, current, and frequency output from the distributed micro sources are not compatible with the large power grid, making a direct connection impossible. Therefore, it is generally necessary to use a voltage inverter to convert the power output of the micro sources into power frequency alternating current before it can be connected to the grid. By designing a suitable inverter control strategy within the allowed input DC voltage, the inverter's output voltage, current, and frequency can be adjusted. There are three commonly used inverter control methods: constant

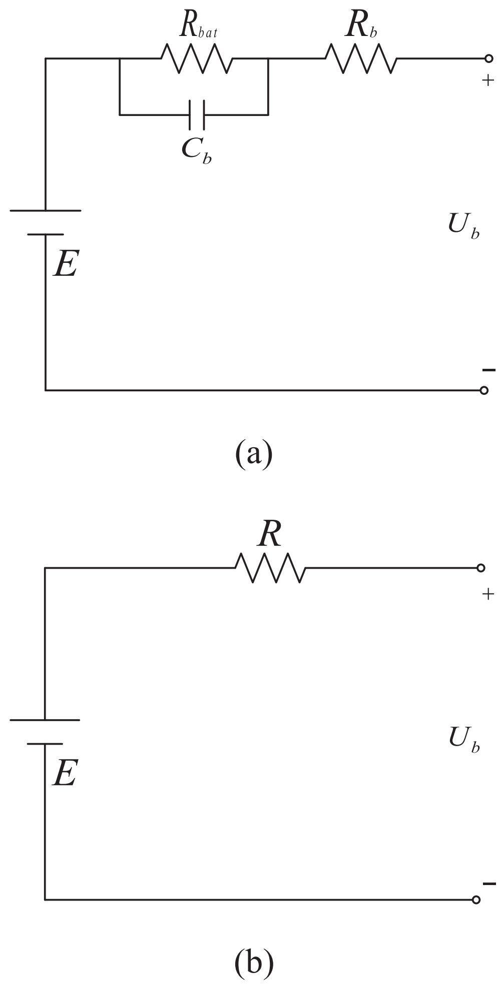

Figure 6. Battery equivalent circuit.

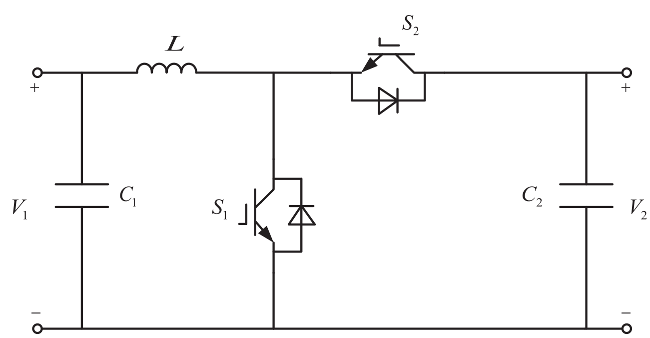

Figure 7. Bidirectional Buck/Boost.

power control, constant voltage, and constant frequency control (V/f control), and droop control.

Constant power control, also known as PQ control, is a control mode where the inverter adjusts its output active power and reactive power based on given reference values for active power and reactive power in the system. Constant voltage constant frequency control, known as V/f control, is a control mode where each micro-source inverter is adjusted

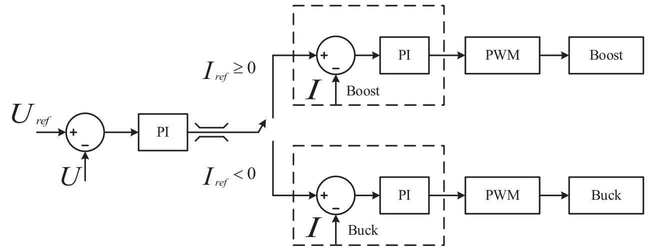

Figure 8. Control block diagram of bidirectional DC/DC converter.

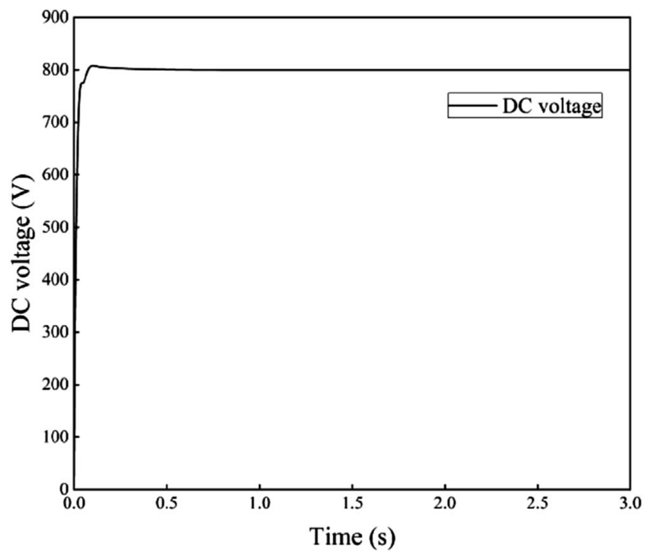

Figure 9. Output voltage of bidirectional DC/DC converter.

to ensure that the output voltage and frequency match the given reference values, without considering the changes in the micro-source's output power. The main objective of V/f control is to maintain the stability of the microgrid system's output voltage, frequency, and amplitude within a certain range, even when the external environment changes. The Droop Control method regulates the output voltage, frequency, and power of the inverter, similar to the primary frequency modulation of traditional power system generator sets.

Since the article focuses on an off-grid microgrid system, V/f control is chosen for the main inverter, while PQ control is selected for the secondary inverter. The main circuit topology of the off-grid inverter is illustrated in Figure 10.

Where, V_{dc} is the DC bus voltage input by the inverter, C_{dc} is the support capacitance of the DC side of the inverter, $S_1 \sim S_6$ is the IGBT switching tube, L_f and R_f are the AC filter inductor and its series equivalent resistance, C_f is AC filter capacitor, i_L is the inductor current of AC filtering, V_N is the output phase voltage of the inverter (N=A, B, and C).

L_f and C_f constitute the LC filter of the off-grid inverter, and the parameters are based on the equations (12) and (13) which are shown in [24].

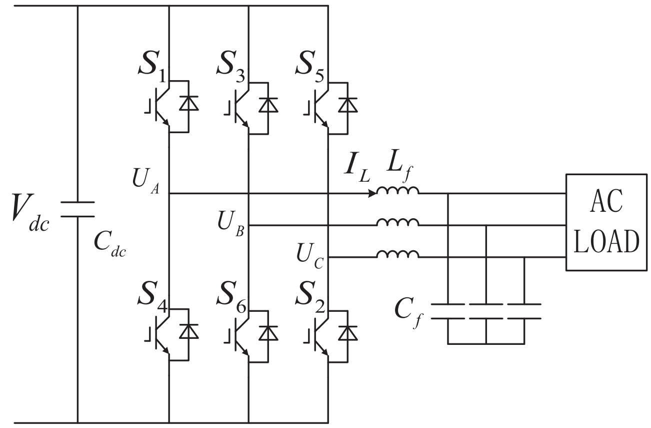

Figure 10. Inverter.

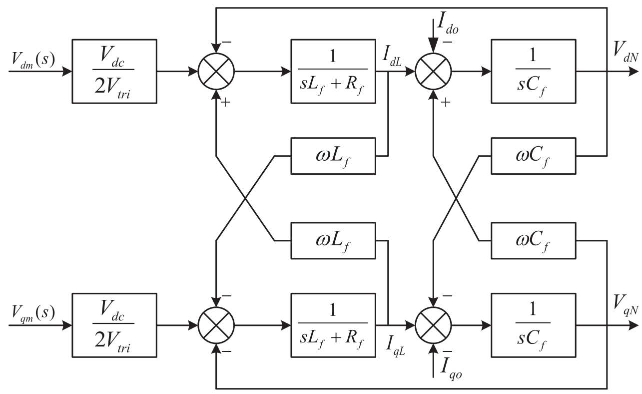

Figure 11. Mathematical model structure of inverter in synchronous rotating coordinate system.

$$L_{max} = \frac{\lambda_v v_o}{\omega_0 I} \tag{12}$$

$$C_{max} = \lambda_C \frac{S_N}{6\pi f_0 v_o^2} \tag{13}$$

Where λ_v is voltage to output phase voltage ratio that is generally taken as 5%, v_o is Root Mean Square (RMS) value the inductor inverter phase voltage, ω_0 is fundamental angular frequency, I is RMS value of inductor current, λ_C is the ratio of reactive power introduced by the capacitor to the rated output power that is typically taken as 6% in this case, S_N is inverter capacity and f_0 is fundamental angular frequency.

A three-phase inverter can be controlled in different coordinate systems, including the stationary three-phase coordinate system (abc coordinate system), stationary two-phase coordinate system ($\alpha\beta$ coordinate system), and synchronous rotating two-phase coordinate system (dq coordinate system). In the abc coordinate system, the control is direct but requires separate control of the three phases. In the $\alpha\beta$ coordinate system, the control is relatively simplified compared to the abc coordinate system, but the controlled variables are still sinusoidal signals. In the dq coordinate system, the control variables are transformed into easily controllable DC signals, simplifying the design of control algorithms and controllers. According to [21], the expression for a three-phase inverter in the dq coordinate system, as shown in Figure 10, is as follows:

$$\begin{cases} C_f \dot{v}_{dN} - \omega C_f v_{qN} = i_{dL} - i_{do} \\ C_f \dot{v}_{qN} - \omega C_f v_{dN} = i_{qL} - i_{qo} \\ L_f i_{dL} - \omega L_f i_{qL} = -v_{dN} - R_L i_{dL} + \frac{V_{dm}(t)}{2V_{tri}} V_{dc} \\ L_f i_{qL} + \omega L_f i_{dL} = -v_{qN} - R_L i_{qL} + \frac{V_{qm}(t)}{2V_{tri}} V_{dc} \end{cases} \tag{14}$$

Where L_f and R_f are the AC filter inductor and its series equivalent resistance, C_f is AC filter capacitor, i_{dL} is the inductor current on d-axis while i_{qL} is on q-axis, i_{do} is the output current on d-axis while i_{qo} is on q-axis, v_{dN} is the capacitor voltage on d-axis while v_{qN} is on q-axis, $V_{dm}(t)$ is the instantaneous value of the modulation waveform on d-axis while $V_{qm}(t)$ is on the q-axis, V_{tri} is the amplitude of the triangular carrier wave, V_{dc} is DC voltage, ω is fundamental angular frequency. According to equation (14), the structure of the model can be obtained, as shown in Figure 11 [24].

The controlled object in this case is the mathematical model of a three-phase inverter in the synchronous rotation coordinate system. It becomes apparent that the d-axis and q-axis components exhibit coupling issues. For example, the d-axis component is influenced by the inductance current and output voltage of the q-axis, and vice versa, the q-axis component is affected by the d-axis component. This coupling relationship makes it nearly impossible for each input to produce an output unaffected by the other, presenting challenges in system control. Therefore, it becomes necessary to find a solution to eliminate this cross-coupling. A common approach to address this is through the use of feedforward decoupling, as illustrated in Figure 12 [24].

The block diagram in Figure 14 illustrates a feedforward decoupling configuration, which serves as an example of a double-loop control system with the voltage outer loop and the inductor current inner loop. The output voltage of the d-axis and the inductor current of the q-axis are incorporated into the control link to eliminate the coupling with the circuit link. In theory, once decoupling is implemented, the coupled system should be controlled. However, practical applications of feed-forward decoupling are unable to achieve complete decoupling due to limitations in control accuracy. As a result, in cases of low control accuracy, only the decoupling of the current inner loop is considered, or no decoupling scheme is adopted. The output voltage of the inverter by V/f control is shown in Figure 13.

5 Microgrid simulation

5.1 Topology of system

Based on the basic structure and control strategy, the authors conducted simulations to validate the concepts. Firstly, following the description mentioned above, the author will establish a hybrid AC/DC microgrid consisting of photovoltaic generation, energy storage connected to the

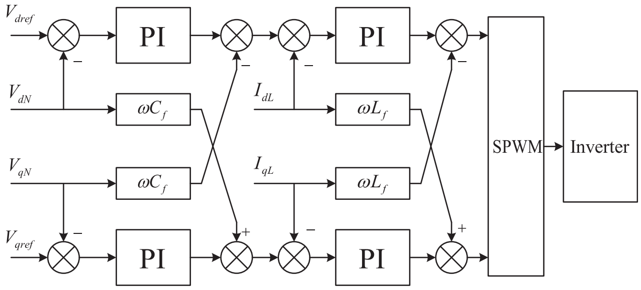

Figure 12. Feed-forward decoupling control.

DC bus, and photovoltaic inverters connected to the AC bus. The connection between the DC bus and AC bus will be achieved through inverters utilizing V/f control. The photovoltaic generation will serve as the power source, while the energy storage system will maintain the voltage of the DC bus. To save time, this simulation will utilize lumped parameters, where each subsystem represents a group of series/parallel subsystems. Additionally, the loads will be simplified, with a single load connected to the AC/DC bus interface. Considering the construction environment of the Sichuan-Tibet Railway, situations requiring island operation may arise. Hence, the author will use the DC side output to represent the DC bus and the AC side output to represent the AC bus, simulating typical operating conditions of an off-grid microgrid to verify the performance of the power sources and inverters. The main circuit topology is depicted in Figure 14.

Also, there is a single photovoltaic array connected to the inverter. It represents the process of the photovoltaic array in a hybrid AC/DC microgrid being connected to the AC bus in close proximity. According to the project requirements, a specific work face of Section 10 of the Sichuan-Tibet Railway plans to use 1272 monocrystalline silicon photovoltaic panel modules with a total capacity of 699.6 kW. However, the simulations in this article only simulate a specific work point with a total capacity of 170 kW of photovoltaic.

5.2 Energy management strategy

To accomplish energy management in the construction area of the Sichuan-Tibet Railway microgrid, this article proposes a time-period-controlled energy management strategy. The article simulates four time periods: night when the photovoltaic system is not operational, morning when the photovoltaic system output is insufficient, noon when the photovoltaic output is high but the load is also significant, and afternoon when the photovoltaic output decreases but the load is relatively lower. The energy relationships during the four time periods should satisfy the following conditions:

$$\forall t,\ P_{PV} + P_{Bat} = P_{load.dc} + P_{load.ac} \tag{15}$$

$$\forall t,\ P_{PV.min} \leq P_{PV} \leq P_{PV.max} \tag{16}$$

$$\forall t,\ P_{Bat.min} \leq P_{Bat} \leq P_{Bat.max} \tag{17}$$

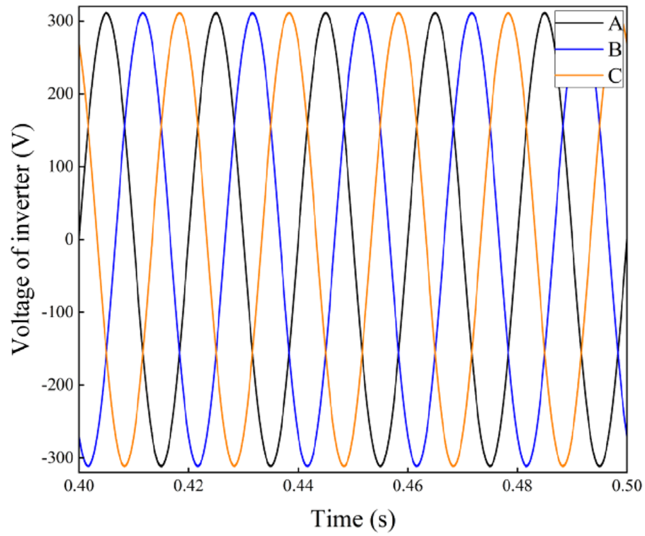

Figure 13. Output voltage of inverter.

$$\forall t,\ 0.1 \leq SOC_t \leq 0.9 \tag{18}$$

The process of energy management strategy involves determining the current time period state of the system, determining the power output for each component based on the current state, and scheduling the system accordingly.

In the first time period, equation (15) is equivalent to

$$\forall t_1,\ P_{Bat} = P_{load.dc} + P_{load.ac} \tag{19}$$

In the second time period, equation (15) is equivalent to

$$\forall t_2,\ P_{PV} + P_{Bat} = P_{load.dc} + P_{load.ac} \tag{20}$$

and

$$\forall t_2,\ P_{PV} < P_{load.dc} + P_{load.ac},\ P_{Bat} > 0 \tag{21}$$

In the third time period, equation (15) is equivalent to

$$\forall t_3,\ P_{PV} + P_{Bat} = P_{load.dc} + P_{load.ac} \tag{22}$$

and

$$\forall t_3,\ P_{PV} > P_{load.dc} + P_{load.ac},\ P_{Bat} < 0 \tag{23}$$

In the fourth time period, equation (15) is equivalent to

$$\forall t_4,\ P_{PV} + P_{Bat} = P_{load.dc} + P_{load.ac} \tag{24}$$

and

$$\forall t_4,\ P_{PV} > P_{load.dc} + P_{load.ac},\ P_{Bat} < 0 \tag{25}$$

5.3 Simulation of system

Based on the topology shown in Figure 14 and energy management strategy, the author conducted simulations of electric equipment charging in the construction area of the Sichuan-Tibet Railway during the night, morning, noon, and afternoon.

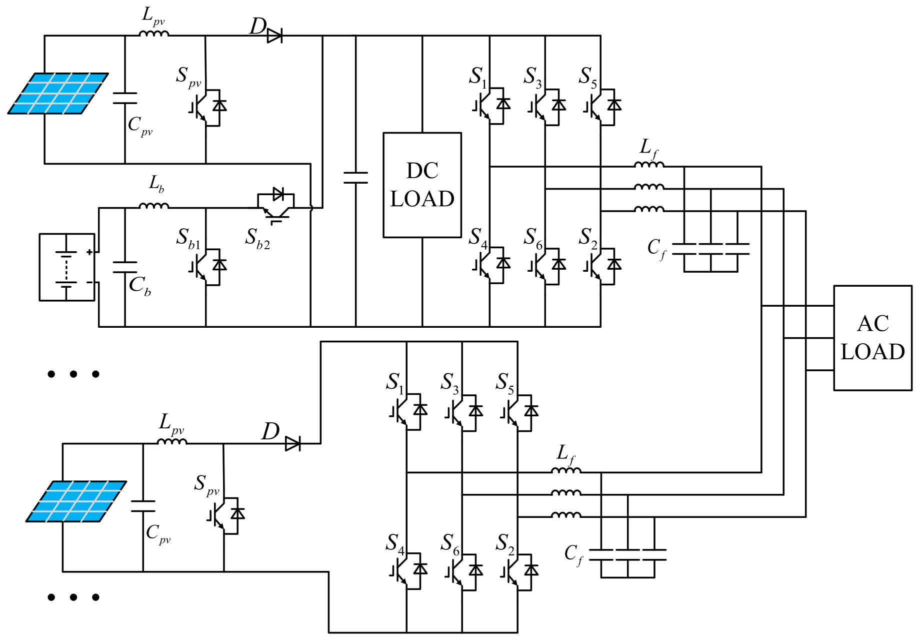

Figure 14. Topology of system.

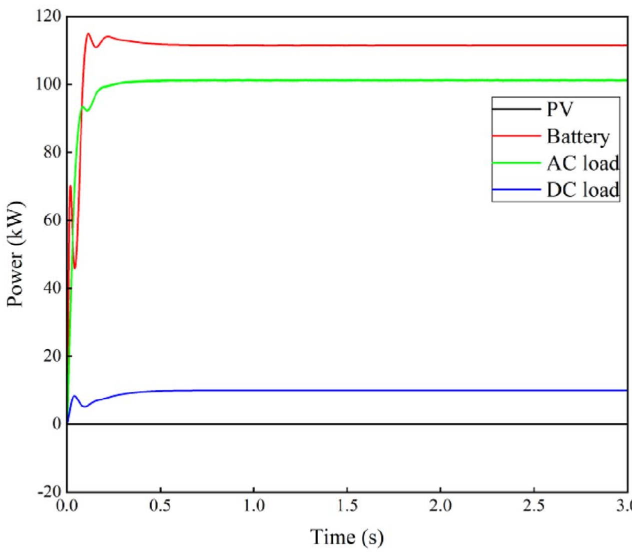

Figure 15. Power flow at night.

During the night, the photovoltaic panels cannot generate electricity, and the energy is obtained from the energy storage system. The electric equipment is not in operation, and slow AC charging can be used. The main load is the AC load. The AC load is set to 100 kW and the DC load can be ignored but still set to 10 kW. The energy distribution is shown in Figure 15.

In the morning, the solar irradiation is not high, and the temperature is not high either. The electricity generated by the photovoltaic panels may not be sufficient to meet the charging demand. Considering that some electric equipment has been in operation for a certain period of time, it needs to be charged at a certain time in the morning. Fast DC charging should be chosen at this time. The AC load is considered as the regular load, with a larger DC load and a smaller AC load. The power from the photovoltaic panels is 70 kW, and the DC load is set to 80 kW. The AC load is set to 10 kW, which represents the regular load of the construction area. The power distribution is shown in Figure 16.

At noon, the solar irradiation is the strongest, and the temperature is the highest. Under normal circumstances, the electricity generated by the photovoltaic panels is sufficient to maintain the operation of the entire microgrid. Any excess energy will be stored in the energy storage system. The workers rest at noon and the regular load increases. The electric equipment, after working in the morning, needs to be charged. However, the rest time at noon is short, so fast DC charging is still chosen, resulting in a larger DC load. The power from the photovoltaic panels is 165 kW, the DC load is set to 120 kW and the AC load is set to 15 kW, which increases during the workers' rest period. The power distribution is shown in Figure 17.

In the afternoon, the solar irradiation is sufficient, and the temperature is relatively high. The electric equipment is in operation, with a smaller DC load and a regular AC load. Most of the energy generated by the photovoltaic panels is stored in the energy storage system. At this time, the power from the photovoltaic panels is 80 kW. The DC load is ignored, the AC load is set to 10 kW, and the DC load is set to 40 kW. Any excess energy will be stored in the energy storage system. The power distribution is shown in Figure 18.

Four sets of simulations were studied in this article. It can be observed that during the night, the photovoltaic system does not operate, and the power balance is maintained by the energy storage system. In the morning, when simulating low photovoltaic power generation, the system relies

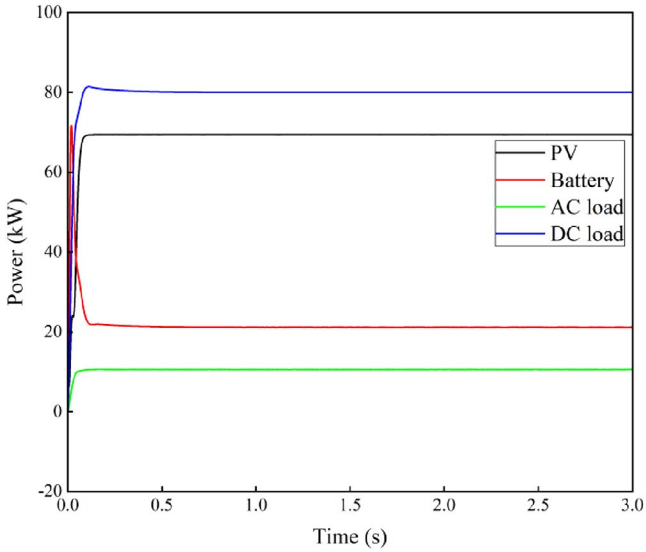

Figure 16. Power flow in the morning.

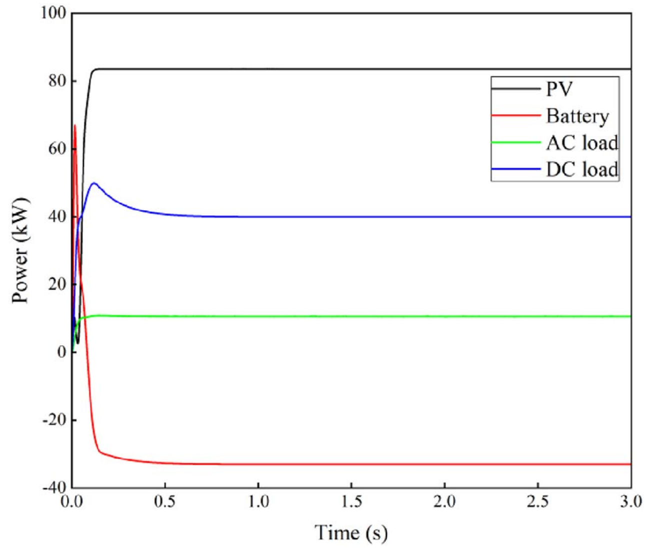

Figure 18. Power flow in the afternoon.

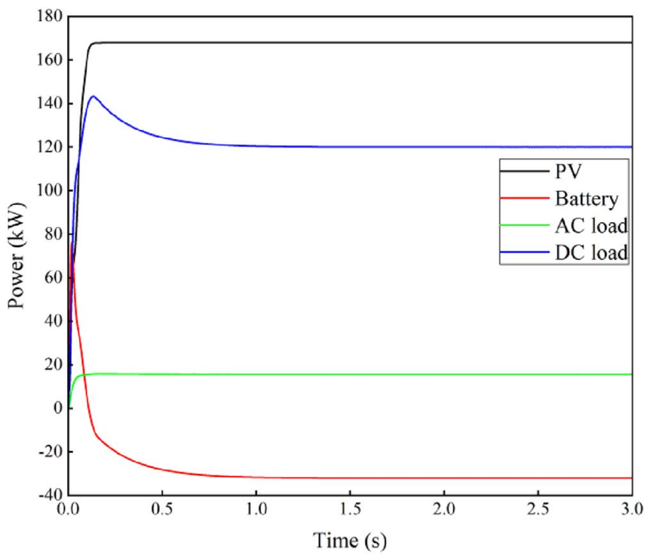

Figure 17. Power flow at noon.

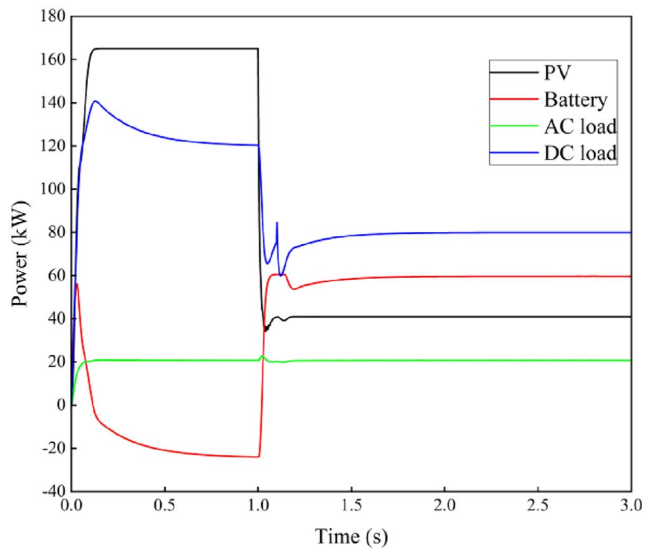

Figure 19. Power flow of PV fault and load shedding.

on both photovoltaic power generation and the energy storage system to supply power and maintain power balance. At noon, when simulating the strongest sunlight, the photovoltaic system supplies power to both the energy storage system and the load. In the afternoon, the intensity of sunlight decreases but still remains relatively high. Due to the reduced load, the photovoltaic system is still able to meet the load demand and excess energy is stored in the energy storage system.

Moreover, the researchers simulated a typical fault scenario, a sharp drop in photovoltaic power generation. At noon, the power of the PV power generation is 165 kW, the DC load power is 120 kW, and the AC load power is 20 kW. Assuming that the maximum charge and discharge power of the energy storage device is 60 kW, when the simulation time is 1 s, the power of the PV power generation drops to 40 kW for some reasons, then the energy storage device switches from the charging state to the discharge state, but it can't meet the load demand. After detecting the corresponding signal, the DC load is properly shed to maximize the balance between supply and demand. The detailed information is shown in Figure 19.

6 Conclusion

This article combines the concept of microgrids with green construction and investigates the establishment of a microgrid in the construction area of the Sichuan-Tibet Railway to power electric equipment. Through comparative analysis, it is found that an AC/DC microgrid is more suitable for the construction area scenario. This article proposes a time-period-controlled energy management strategy, aiming to ensure the smooth operation of the microgrid during different time periods. By comparing with the case presented in [9], the proposed microgrid and energy management strategy effectively coordinate the photovoltaic system and energy storage system to provide power to electric devices during different time periods.

Utilizing the abundant solar irradiation resources and energy storage systems in the construction area of the Sichuan-Tibet Railway, this article achieves green construction. However, the content of this article only considers one working face and has not been extended to the entire construction area. The proposed energy management strategy is accurate and efficient for different time periods but requires substantial communication requirements to integrate operational information.

In the future, the research people plan to promote the concepts and energy management strategies proposed in this article and focus on studying energy management strategies for a cluster of microgrids covering the entire construction area. Additionally, they will work on retrofitting the microgrid after completion of construction to ensure power supply to electric locomotives.

Conflicts of interest

The authors declare no conflict of interest.

References

1. Ibáñez-Rioja A., Järvinen L., Puranen P., Kosonen A., Ruuskanen V., et al. (2023) Off-grid solar PV–wind power–battery–water electrolyzer plant: simultaneous optimization of component capacities and system control, *Appl. Energy* **345**, 1, 121277.
2. Su R., Gu Q., Wen T. (2014) Optimization of high-speed train control strategy for traction energy saving using an improved genetic algorithm, *J. Appl. Math.* **2014**, 507308.
3. Zhang K., Huang W., Hou X., Xu J., Su R., Xu H. (2021) A fault diagnosis and visualization method for high-speed train based on edge and cloud collaboration, *Appl. Sci.* **11**, 3, 1251.
4. Shen Y., Gao Y., Hu Y., Yao X., Yu W., et al. (2023) Spatial and temporal distribution characteristics of solar energy resources in Tibet, *Energy Eng.* **121**, 1, 43–57.
5. Kilic H. (2023) Distributed cooperative fault tolerant optimal active power control in AC microgrid, *ISA Trans.* **142**, 98–111.
6. Widjaja R., Asrol M., Agustono I., et al. (2023) State of charge estimation of lead acid battery using neural network for advanced renewable energy systems, *Emerg. Sci. J.* **7**, 3. http://dx.doi.org/10.28991/ESJ-2023-07-03-02.
7. Uddin M., Mo H., Dong D., Elsawah S., Zhu J., et al. (2023) Microgrids: a review, outstanding issues and future trends, *Energy Strat. Rev.* **49**, 101127.
8. Saeed M.H., Wang F., Kalwar B.A., Iqbal S. (2021) A review on microgrids' challenges & perspectives, *IEEE Access* **9**, 166502–166517.
9. Wan L. (2018) Current situation and case analysis of intelligent distributed photovoltaic microgrid in plateau and cold region, *Tibet Sci. Technol.* **9**, 16–20. (In Chinese).
10. Wang Y. (2018) Research review on intelligent distributed photovoltaic microgrid in plateau and cold region, *Tibet Sci. Technol.* **6**, 22–30. (In Chinese).
11. Cao T. (2016) *The optimization design of solar micro grid in the mountain areas of high altitude*, North China Electric Power University, China. (M.S. Thesis).
12. Yang H. (2023) Research on power and energy storage capacity of constant output power "PV+Energy Storage" system in micro-grid, *Sol. Energy* **9**, 30–37. (In Chinese).
13. Wu J. (2019) Design of DC microgrid control system, *Magaz. Equip. Mach.* **4**, 12–16. (In Chinese).
14. Geng Y., Zhong Y., Li Q. (2017) Design of hardware circuit for bidirectional DC–DC controller in DC micro-grid energy storage system, *Mar. Electr. Electron. Technol.* **37**, 7, 44–47. (In Chinese).
15. Guo F., Wang L., Zhang D., Xu Q. (2020) Distributed voltage restoration and current sharing control in islanded DC microgrid systems without continuous communication, *IEEE Trans. Industr. Electron.* **67**, 4, 3043–3053.
16. Eghtedarpour N., Farjah E. (2014) Power control and management in a hybrid AC/DC microgrid, *IEEE Trans. Smart Grid* **5**, 3, 1494–1505.
17. Pragya Thakur R. (2022) A review of architecture and control strategies of hybrid AC/DC microgrid, in: *2022 International Conference on Intelligent Controller and Computing for Smart Power (ICICCSP)*, Hyderabad, India, pp. 1–5.
18. Xue S. (2016) *Research on coordination control of a hybrid AC/DC microgrid*, Southeast University, China. (M.S. Thesis).
19. Zhu Y., Tang Q., Jia L. (2017) New hybrid AC/DC microgrid topology and its reliability analysis, *Electr. Power Constr.* **38**, 9, 81–87. (In Chinese).
20. Liu D. (2016) *Research on operation control strategy of dual mode PV-storage microgrid system*, Beijing Jiaotong University, China. (M.S. Thesis).
21. Balal A., Pakzad Y., Demir A., et al. (2023) Forecasting solar power generation utilizing machine learning models in Lubbock, *Emerg. Sci. J.* **7**, 4. http://dx.doi.org/10.28991/ESJ-2023-07-04-02.
22. Prasetyo D., Budiana P., Praowo R., Arifin Z. (2023) Modeling Finned thermal collector construction nanofluid-based Al2O3 to enhance photovoltaic performance, *Civil Eng. J.* **9**, 12. http://dx.doi.org/10.28991/CEJ-2023-09-12-03.
23. Xi Z. (2023) *Research on bidirectional DC/DC parallel operation control strategy of DC microgrid*, Lanzhou University of Technology, China. M.S. Thesis.
24. Lan Z. (2022) *Research on control strategy of off-grid voltage source inverter.* M.S. Thesis. Beijing Jiaotong University, China.